

Structure and Cell Wall Cleavage by Modular Lytic Transglycosylase MltC of *Escherichia coli*

Cecilia Artola-Recolons,^{1,†} Mijoon Lee,^{1,‡} Noelia Bernardo-García,[†] Blas Blázquez,[‡] Dusan Hesek,[‡] Sergio G. Bartual,[†] Kiran V. Mahasenan,[‡] Elena Lastochkin,[‡] Hualiang Pi,[‡] Bill Boggess,[‡] Kathrin Meindl,^{§,||} Isabel Usón,^{§,||} Jed F. Fisher,[‡] Shahriar Mobashery,*[‡] and Juan A. Hermoso*,[†]

[†]Department of Crystallography and Structural Biology, Inst. Química-Física "Rocasolano", CSIC, Serrano 119, 28006 Madrid, Spain

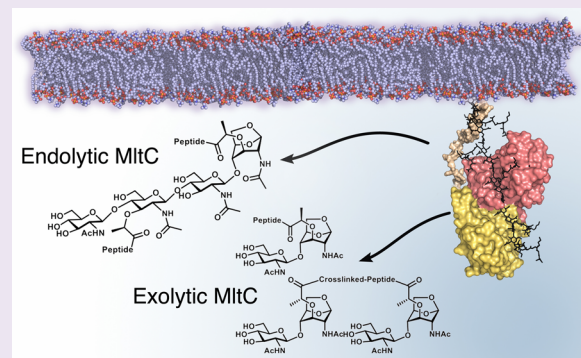
[‡]Department of Chemistry and Biochemistry, Nieuwland Science Hall, University of Notre Dame, Notre Dame, Indiana 46556, United States

[§]Instituto de Biología Molecular de Barcelona, CSIC, Baldiri Reixach 13, 08028 Barcelona, Spain

^{||}ICREA (Institució Catalana de Recerca y Estudis Avançats), Passeig Lluís Companys 23, 08010 Barcelona, Spain

Supporting Information

ABSTRACT: The lytic transglycosylases are essential bacterial enzymes that catalyze the nonhydrolytic cleavage of the glycan strands of the bacterial cell wall. We describe here the structural and catalytic properties of MltC, one of the seven lytic transglycosylases found in the genome of the Gram-negative bacterium *Escherichia coli*. The 2.3 Å resolution X-ray structure of a soluble construct of MltC shows a unique, compared to known lytic transglycosylase structures, two-domain structure characterized by an expansive active site of 53 Å length extending through an interface between the domains. The structures of three complexes of MltC with cell wall analogues suggest the positioning of the peptidoglycan in the active site both as a substrate and as a product. One complex is suggested to correspond to an intermediate in the course of sequential and exolytic cleavage of the peptidoglycan. Moreover, MltC partitioned its reactive oxocarbenium-like intermediate between trapping by the C6-hydroxyl of the muramyl moiety (lytic transglycosylase activity, the major path) and by water (muramidase activity). Genomic analysis identifies the presence of an MltC homologue in no less than 791 bacterial genomes. While the role of MltC in cell wall assembly and maturation remains uncertain, we propose a functional role for this enzyme as befits the uniqueness of its two-domain structure.



A critical task for bacteria is the preservation of the integrity of their cell wall. This task summons numerous enzymes to simultaneously control the elongation, the remodeling, the puncture (to accommodate protein access to the exterior of the bacterium), and the cleavage of its cell wall following cell division. Just how critical this task is for the bacterium may be measured by the extensive ensemble of antibiotic classes that target both the cell wall structure and the enzymes involved in its preservation.¹ The bacterial cell wall (also known as the sacculus) is a complex cross-linked polymer.^{2,3} Its building unit is the peptidoglycan, comprising a repeating disaccharide *N*-acetylglucosamine-*N*-acetylmuramic acid (NAG-NAM) glycan strand, and a uniquely bacterial pentapeptide stem (in most Gram-negative bacteria: L-Ala-D-γ-Glu-meso-DAP-D-Ala-D-Ala, where DAP is the abbreviation for diaminopimelate) appended to the NAM saccharides. In the mature peptidoglycan, the glycan strands are cross-linked by a transpeptidation reaction, wherein one stem is joined to the free amine of the DAP residue of a neighboring stem.

Among the most interesting enzymes contributing to the cell wall integrity of Gram-negative bacteria (including many pathogens such as *Escherichia coli*, *Pseudomonas aeruginosa*, *Salmonella* sp., *Helicobacter pylori*, and *Neisseria gonorrhoeae*) are the lytic transglycosylases (LTases). The LTases nonhydrolytically cleave the NAM-NAG glycosidic bond, which entails the formation of a reactive oxocarbenium species upon the breakage of the glycosidic bond. The reactive oxocarbenium species is formed at the anomeric carbon of the NAM unit, and it entraps the NAM C6-hydroxyl to form a 1,6-anhydromuramic terminus (Figure 1A). The LTases are implicated in critical events: in the late step of cell wall biosynthesis, in peptidoglycan recycling, in second-messenger formation to control the expression of β-lactamases as antibiotic-resistance enzymes, in the release of peptidoglycan-derived pathogen-associated molecular patterns as a virulence mechanism, in

Received: June 3, 2014

Accepted: July 2, 2014

Published: July 2, 2014

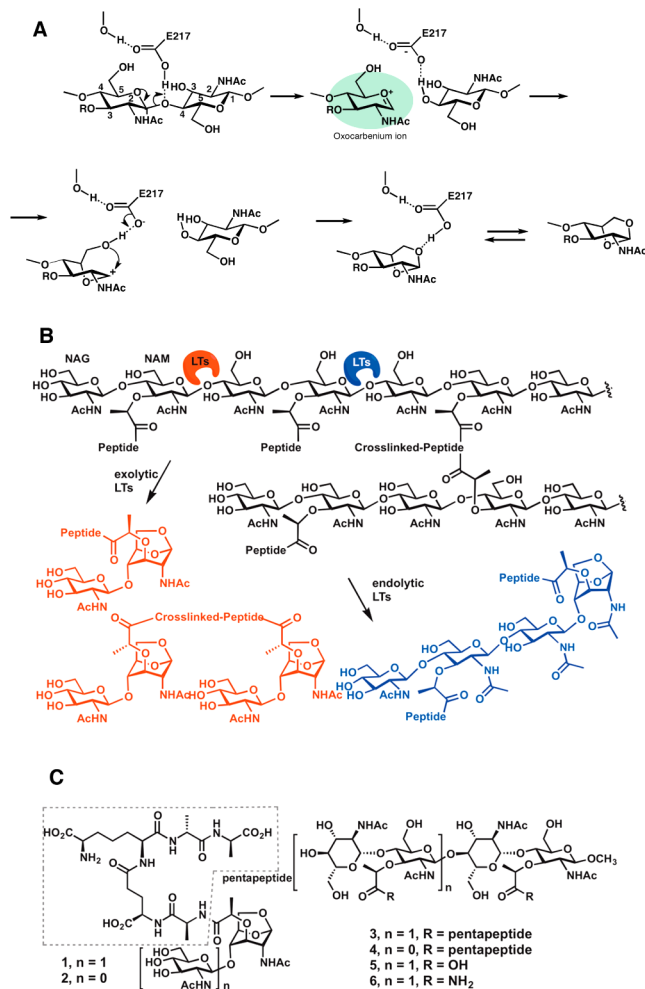


Figure 1. (A) Proposed stepwise process in turnover of substrate by lytic transglycosilases. (B) A sampling of the reactions by the endolytic and exolytic activities of MltC. (C) The six synthetic compounds used in the present study.

peptidoglycan puncturing to accommodate multiprotein structures such as the anchoring of the flagella, and in cell division. The LTase family of *Escherichia coli* is arguably the best studied and consists of seven enzymes (annotated as MltA, MltB, MltC, MltD, MltE, MltF, and Slt70). The first six are membrane-bound (to the inner leaflet of the outer membrane) while Slt70 is a soluble enzyme found within the periplasmic space.^{4,5} The number of LTases within each bacterial species is variable, and as studied within the *E. coli* family, the activity of one can compensate for the loss of activity of others. Indeed, a viable *in vitro* planktonic *E. coli* phenotype is obtained following deletion of all of the LTases save MltF (but one is not obtained upon deletion of all seven).⁶

Some measure of the function of each LT is now emerging from the combination of genomic and structural analyses, phenotype characterization upon genetic deletion, and the use of HPLC-MS analysis of the peptidoglycan fragments (muropeptides) obtained upon digestion of the whole peptidoglycan sacculus accomplished by each individual LTase family member. Evaluation of the *E. coli* family using this latter assay method has enabled initial assignments within the family of those LTases that preferentially perform endolytic (cleavage in the middle of the peptidoglycan) and exolytic (cleavage at the terminus) reactions (Figure 1B), and as well

those that show preference for the presence (or absence) of cross-linked stems.⁷ MltC has a preferential exolytic activity; however, experiments digesting the sacculus revealed that a 0.5% of the activity of MltC is endolytic.⁷ An understanding of the structural bases for these preferences is just now emerging. Notwithstanding strong structural conservation within the catalytic domains of LTases of *E. coli*, an overall structural comparison of the X-ray structures for soluble constructs of MltA,⁸ MltB,⁹ MltE,^{10,11} and Slt70¹² show each to be distinct. While the smallest protein is MltE (corresponding to the spare catalytic domain) the others have additional domains of unknown function(s).⁴ Here, we present the structure of a soluble construct of *E. coli* MltC. The two-domain MltC structure—an N-terminal structural domain and a C-terminal catalytic domain—is unique when compared to the structures of the four *E. coli* LTases solved previously. Moreover, emerging from these studies is a mechanistic understanding to explain catalysis by MltC and a hypothesis for the functional role of the enzyme within the bacterium.

RESULTS AND DISCUSSION

The *mltC* gene corresponding to amino acids 19–359 of the native enzyme was cloned. This construct excludes the cysteine residue (Cys17) that would be S-lipidated by transfer of the nascent protein to a phosphatidylglycerol molecule in the inner leaflet of the outer membrane. Cloning from residue 19 ensured a soluble recombinant protein, which was purified to homogeneity. The apo MltC was crystallized both as the wild type and as a catalytically impaired E217Q variant (used just for crystallization of all complexes). Residue Glu217 is the required proton donor to the scissile glycosidic bond that leads to the reactive oxocarbenium species; hence, its conservative mutation to glutamine abrogates its catalytic activity. These crystals were soaked with various synthetic peptidoglycan derivatives corresponding to both peptidoglycan substrate analogs and LTase reaction products (compounds 1–6; Figure 1C).^{13–16} Among these structures are three tetrasaccharides (compound 3 with peptide stems and compounds 5 and 6 without) as mimetics of the longer-chain peptidoglycan, and a product, compound 1. None of compounds 3–6 was a substrate for MltC. Hence, the minimum length for a substrate of this enzyme must be more than four saccharides. Four structures were solved: apo MltC (2.3 Å resolution), the MltC·1 complex (2.4 Å resolution), the MltC·5 complex (2.1 Å resolution), and the MltC·6 complex (3.0 Å resolution) (Table 1).

Structural determination was performed *de novo* by using Arcimboldo.^{17,18} The asymmetric unit of each crystal contained two protein molecules, with each presenting nearly identical structures as assessed by a backbone root-mean-square deviation (rmsd) value of 0.36 Å. Each monomer (Figure 2) parses into a novel N-terminal domain (residues 30–182) and a catalytic C-terminal domain (residues 183–359, showing the expected GH23 fold). As the MS analysis for the recombinant protein gives the expected mass value ($M_r = 38\ 495 \pm 4$; predicted mass of $M_r = 38\ 493$) for the amino-acid residues 19–259 construct, residues 19–29 are present but are not seen in the electron density due to disorder (as is also predicted by the DisEMBL server (<http://dis.embl.de/>)). The two domains are intimately linked (Figure 2) by extensive aromatic-zipper (interdigitated aromatic side chains) and polar interactions (Supporting Information Figure S4) shared across an extended interface.

Table 1. Data Collection and Refinement Statistics^a

	MltC	MltC·1 complex	MltC·5 complex	MltC·6 complex
Diffraction Data Statistics				
wavelength (Å)	1.74709	0.87260	0.97948	0.97948
space group	P2 ₁	P2 ₁	P2 ₁	P2 ₁
<i>a</i> , <i>b</i> , <i>c</i> (Å)	49.87, 114.65, 61.40	50.16, 115, 61.28	49.51, 114.33, 61.77	49.21, 112.81, 61.57
α , β , γ	90, 93.46, 90	90, 93.21, 90	90, 93.28, 90	90, 93.52, 90
resolution range (Å)	45.66–2.33 (2.46–2.33)	50.08–2.45 (2.58–2.45)	49.43–2.15 (2.23–2.15)	43.03–2.9 (3.07–2.9)
unique reflections	28559 (2263)	25528 (2539)	37159 (3686)	18454 (2311)
completeness (%)	97.22 (84.21)	100.0 (100.0)	99.68 (99.84)	99.8 (99.8)
redundancy	3.6 (3.2)	3.7 (3.7)	5.4 (5.0)	4.2 (4.0)
<i>R</i> _{merge}	0.12 (0.62)	0.18 (0.94)	0.11 (0.54)	0.16 (0.40)
avg. <i>I</i> / <i>σ</i> (<i>I</i>)	8.64 (1.8)	7.2 (1.5)	6.6 (1.9)	3.6 (2.2)
Refinement Statistics				
resolution range (Å)	45.66–2.33	45.92–2.45	49.43–2.15	14.93–2.9
<i>R</i> _{work} / <i>R</i> _{free}	0.19/0.26	0.19/0.25	0.19/0.27	0.16/0.25
No. Atoms				
protein	5214	5154	5154	5154
water	104	102	203	48
ligand		69	168	136
B-Factor (Å ²)				
protein	43.30	43.60	42.50	36.70
water	37.40	32.50	37.30	24.50
ligand		93.90	36.10	44.20
Root-Mean-Square Deviations				
bond length (Å)	0.011	0.015	0.013	0.030
bond angles (deg)	1.26	1.38	1.21	2.05
Ramachandran favored/outliers (%)	98.0/0.3	98.0/0.0	96.0/0.46	94/0.3
residues in the AU	660	654	654	654
PDB code	4C5F	4CHX	4CFP	4CFO

^aValues between parentheses correspond to the highest resolution shells.

According to the Dali Server¹⁹ the closest structural homologues of the catalytic domain of MltC are *E. coli* MltE^{10,11} and the catalytic domain of *E. coli* Slt70¹² (Supporting Information Figure S2). The N-terminal domain of MltC does not have any structural precedent and is comprised of a five-stranded antiparallel β -sheet and a 20 amino-acid-long α helix (α_{N1}) on one side, and two α helices (α_{N2} and α_{N3}) on the other (Figure 2A and Supporting Information S3).

Although not hydrolytic enzymes (but possessing a lysozyme fold), the LTase active site adopts the naming convention for hydrolytic enzymes, wherein the subsites flanking the scissile bond in the substrate are designated positions $-i$ (the “non-reducing” end), and through $+j$ in the opposite direction. The saccharide units immediately flanking the scissile glycosidic bond are designated as positions -1 (occupied by the NAM saccharide) and $+1$ (occupied by the NAG saccharide). As seen in the MltC·5 and MltC·6 complexes, the catalytic domain of MltC has an extended (approximately 23 Å in length) recognition site for the peptidoglycan backbone (Figure 2B). Moreover, this expansive active site merges seamlessly into a second peptidoglycan-binding site found in the second domain, extending the active site by an additional ~30 Å. The contiguous concavity of the catalytic and of the N-terminal domains defines an extended groove (of approximately 53 Å total length) capable of accommodating at least nine saccharide residues (Figure 2A). The length of this groove implicates also an endolytic activity for MltC, as is indeed observed in reactions with the sacculus.⁷ The seat of the reaction is roughly in the middle of the extended peptidoglycan-binding groove.

Crystals of the inactive E217Q mutant were soaked with the tetrasaccharide substrate analogues **5** and **6** resulting in two separate complexes (MltC·5 and MltC·6) each showing excellent electron density and occupying the -1 to -4 subsite positions (Figure 2B and Supporting Information Figures S5–S6). Compounds **5** and **6** are β -methyl glycosides and leave the $+1$ subsite (and beyond) unoccupied. The positions of **5** and **6** nearly superimpose in these complexes (Supporting Information Figure S9). The tetrasaccharides are stabilized by numerous polar interactions (Supporting Information Figures S7–S8), especially from residues R147, D244, R247, K314, and E341, and by three tyrosine residues (Y273, Y281, and Y299). The side-chain of the catalytic Glu217 in the wild-type enzyme has a hydrogen-bond interaction through one of its carboxylate oxygens with Tyr345, while the other oxygen is oriented to the glycosidic oxygen of the substrate surrogate (Supporting Information Figure S10). This interaction is what would be expected for the proton donor to the scissile glycosidic bond. In the inactive Gln217 mutant, this interaction is altered slightly (Supporting Information Figure S10).

We had previously reported that MltC is primarily an exolytic enzyme, removing two saccharides from one terminus of the peptidoglycan with cleavage occurring between the -1 and $+1$ subsites. This exolytic reaction liberates disaccharide **1** as the product of each turnover (Figure 3A). The two products of the reaction occupy the -1 to -4 subsites (the larger peptidoglycan; “product I”) and subsites $+1$ and $+2$ (disaccharide **1**; “product II”), respectively. We soaked crystals of the E217Q mutant with **1** (product II) and determined the

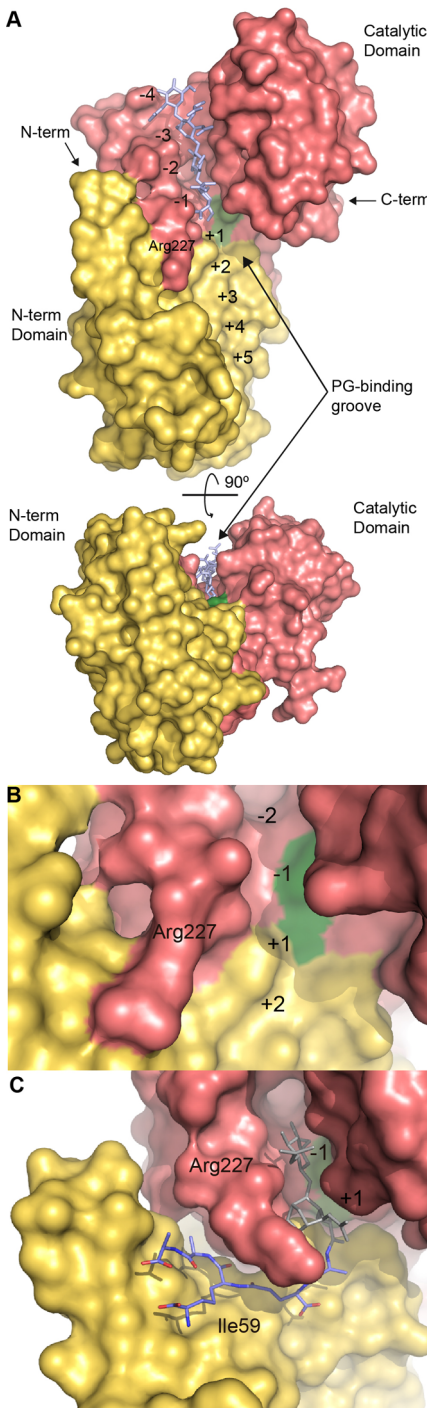


Figure 2. (A) Ribbon representation of MltC with secondary structural elements labeled. The N-terminal domain is colored in yellow and the catalytic domain is colored in pink. These domain colors are retained in all other figures. (B) Molecular surface representation of MltC in complex with tetrasaccharide 5. The position of the catalytic Glu217 (Gln217 in the complex) is in green. The tetrasaccharide 5 sequestered at the peptidoglycan-binding groove is represented in blue capped sticks. The N-terminus, the site of attachment of residues 19–29 and the fatty acyl membrane anchor, which is not seen in the electron density, is indicated by an arrow at 11 o'clock. C) A close-up of the molecular surface of the seat of the catalytic reaction in apo MltC and D) of MltC in complex with 1. The disaccharide portion of the ligand that was modeled computationally is colored in gray sticks.

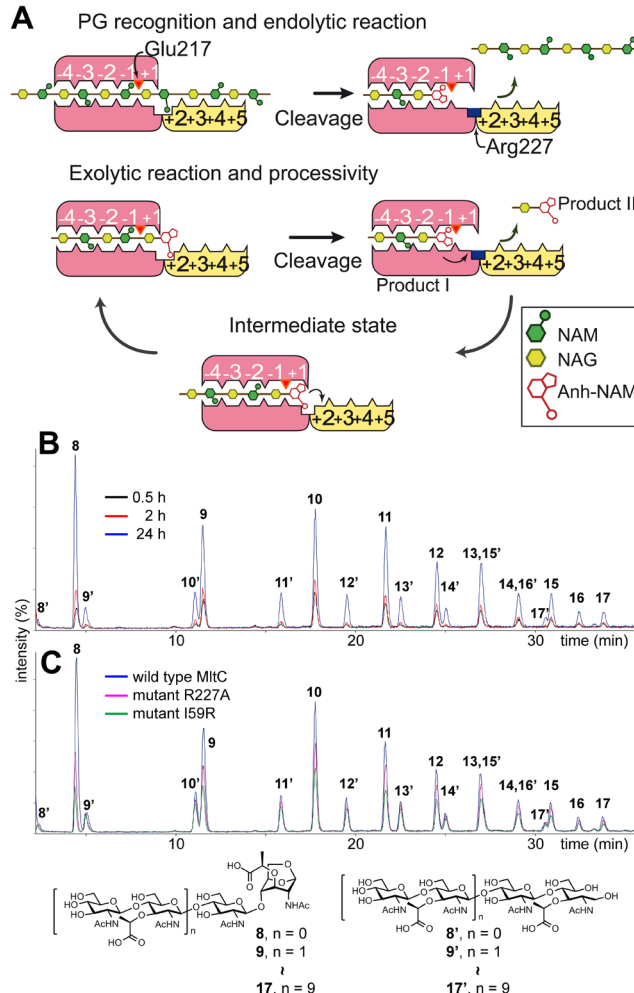


Figure 3. (A) Scheme showing the proposed mechanism for the endolytic and exolytic activities in MltC. (B) The LC/MS extracted-ion chromatograms (EICs) of the reaction products of MltC (C) and of mutants R227A and I59R with the sacculus, followed by that of AmpDh3. Note that the reducing end of the primed products was reduced by sodium borohydride to simplify the chromatogram.

X-ray structure of the resulting complex at 2.4-Å resolution (Figure 2D). The affinity of 1 for the enzyme must be poor, as only the peptide density for compound 1 was clearly seen, with an absence of density for the disaccharide, indicative of mobility of the disaccharide segment within the complex (Supporting Information Figure S11). This finding is explainable for efficient catalysis, as a high affinity for the subsites would result in product inhibition.

The saccharide portion of the ligand was modeled computationally into the X-ray structure for the peptide stem. There is an important observation from the MltC-1 complex: the position of the peptide stem necessitates occupation of the +1 subsite by the 1,6-anhydromuramyl moiety and of the -1 subsite by the N-acetylglucosamine (NAG) (Figure 2D and Supporting Information Figure S12). We verified experimentally that compound 1 is not a substrate for MltC, yet the saccharides in this compound straddle the -1 and +1 subsites in this complex. We assert that this complex is an intermediate state (Figure 3A) in translocation of "product I" forward for another turnover event. The position of Arg227 in these complexes is of special interest with respect to turnover. The side chain of Arg227 aligns with subsites +1 and +2 and is flush

against the protein surface in our two tetrasaccharide complexes and in the apo enzyme (Figure 2B and C). Arg227 defines a portion of the concave saccharide-binding surface of the active site. This residue experiences motion in catalysis. In the complex with **1**, Arg227 has been lifted from the surface of the protein, such that a binding site for the peptide stem of the product **1** is now created (Figure 2D and Supporting Information Figure S13), to which the peptide stem binds. The creation of this peptide-binding pocket and its attendant binding to the substrate peptide stem that exists within the seat of the reaction pulls the entire product **1** (as represented by compound **1**) forward by one “subsite notch” to this intermediary state. In a sense, Arg227 is behaving as a “molecular ratchet” for advancing product **1** for another catalytic cycle. As will be documented below, a mass spectrometry experiment will provide evidence for this assertion.

To document this mechanism, we designed an experiment in which the *E. coli* saccus was first fragmented by MltC, followed by the removal of all peptide stems by the reaction of AmpDh3 peptidase from *Pseudomonas aeruginosa*.^{20,21} AmpDh3 is a peptidoglycan amidase that hydrolyzes the amide bond between the lactyl moiety of muramyl or 1,6-anhydromuramyl moiety and the N-terminal L-Ala of the stem peptide. This processing of the saccus identifies all the soluble products of the MltC reaction without the complication of the variable structures for the stem peptides. Figure 3B shows LC/MS extracted-ion chromatograms (EICs) of reaction products of the wild-type MltC with saccus, followed by the AmpDh3 reaction with different incubation times (0.5, 2, and 24 h). The first peak corresponds to the smallest product, the disaccharide NAG-1,6-anhMur (**8**), and the subsequent peaks to oligomeric products (**9–17**, up to 20 saccharide length for the glycan strand). It is of interest that we also detected products with reducing-end saccharides (compounds **8'–17'**), which are formed when the transient oxocarbenium species (Figure 1A) entraps a water molecule instead of the C6-hydroxyl group of the NAM. Hence, MltC actually partitions the oxocarbenium species between the C6-hydroxyl and water in a ratio of 2.0–18 (Supporting Information Table S1). The fidelity of entrapment of the C6-hydroxyl of the NAM moiety, the hallmark of the LTase reaction, is variable, and depending on the nature of the resulting product, which could indeed be quite poor. The amounts of all products increased as a function of time within the 0.5–24 h monitoring period, as to be expected.

The larger peptidoglycan (“product **1**”) advances to straddle the **-1** and **+1** subsites to initiate catalytic formation of the disaccharide NAG-1,6-anhMur (compound **8**) after each cycle. If the cationic character and the side-chain motion of Arg227 are critical to this translocation of the substrate within the active site, then altering Arg227 (disturbing the “molecular ratchet”) should alter the enzymatic behavior. We cloned two mutant variants of MltC, R227A, and I59R (at the peptide-binding site, Figure 2C and D). The mutant variants were expressed and purified to homogeneity and were analyzed for products release from the saccus as the substrate, as described above for the wild-type MltC (Table 2). The mutant enzymes were less active, as to be expected for an enzyme tampered within the active site. The key observation from this quantitative assay was the relative amount of compound **8** to compounds **9–17**. Compound **8** is the product of sequential-exolytic cleavage of the longer peptidoglycan. Compounds **9–17** are the other turnover products. These products could

Table 2. Turnover of Saccus by the Wild-Type MltC and Its Mutant Variants

product(s)	relative mutational effect ^{a,b}		
	wild-type	R227A	I59R
8	1.0	0.6 ± 0.2	0.4 ± 0.1
9(')–17(')^c	1.0	1.0 ± 0.1	0.7 ± 0.1

^aAmounts as AUC and as percentage of the total EIC. ^bAmounts of products normalized to that of the wild-type MltC. ^cSum of products **9–17** and **9'–17'**.

conceivably dissociate from the enzyme and rebind to the active site. If enzymatic processivity were operative, one would expect that the R227A or I59R mutational effect on the formation of compound **8** should be more significant than that for all of the other products (**9–17** and **9'–17'**). Stated differently, the absence of processivity should reveal the same mutational effect on all products. Our data are consistent with the former and refute the latter possibility (Table 2). Our results indicate a relevant role for Arg227 and the peptide-binding site in translocation of the substrate and are, to our knowledge, the first experimental demonstration of processivity among LTases.

We performed one additional experiment to document the importance of the peptide stems in the peptidoglycan to the catalytic activity of MltC. We isolated compounds **9–17** (mixture of oligomeric saccharides without peptide stems) by liquid chromatography and incubated this glycan mixture with MltC. No change in the glycan strand length was seen. Hence, MltC requires the presence of the peptide stems for its catalysis.

In order to identify if MltC has a preferential activity against soluble or insoluble fractions of the saccus, insoluble saccus was separated after MltC reaction and was subsequently reacted by mutanolysin, which hydrolytically cleaves the glycosidic bond between NAM-NAG of peptidoglycan backbone. This process will reduce complexity originated from polymeric nature of sugar backbone. If there were a reaction by MltC on the insoluble saccus, incubation with mutanolysin would produce more products with anhydroMur than control (mutanolysin alone). Ratio of anhydroMur-containing vs muramic acid-containing products from the mutanolysin digestion of insoluble saccus after MltC was very similar to that of mutanolysin alone after MltC (0.12 and 0.11, respectively). On the contrary, this ratio increases to 26 for soluble portion of saccus after MltC reaction. Therefore, MltC reaction with bacterial saccus is seen mostly in soluble portion, not insoluble portion, of saccus.

The distinguishing structural feature of MltC is its intimate fusion of a catalytic domain with an auxiliary peptidoglycan-binding N-terminal domain both anchored to the membrane through a flexible linker. As there is no structural precedent for the N-terminal domain, its purpose must be surmised by experimentation. One possibility is preferential recognition of longer peptidoglycan strands within the saccus, as the extended 53-Å groove within MltC accommodates it. This observation is supported by superimposing the NMR model of the peptidoglycan²² onto the tetrasaccharides observed in complexes MltC-**5** and MltC-**6**. The resulting model reveals that MltC can accommodate a peptidoglycan of at least nine saccharides in length, and retaining the helical conformation seen in solution for the peptidoglycan²² (Figure 4A). Remarkably, this analysis can be done, provided that the bound strand of peptidoglycan is not cross-linked as the

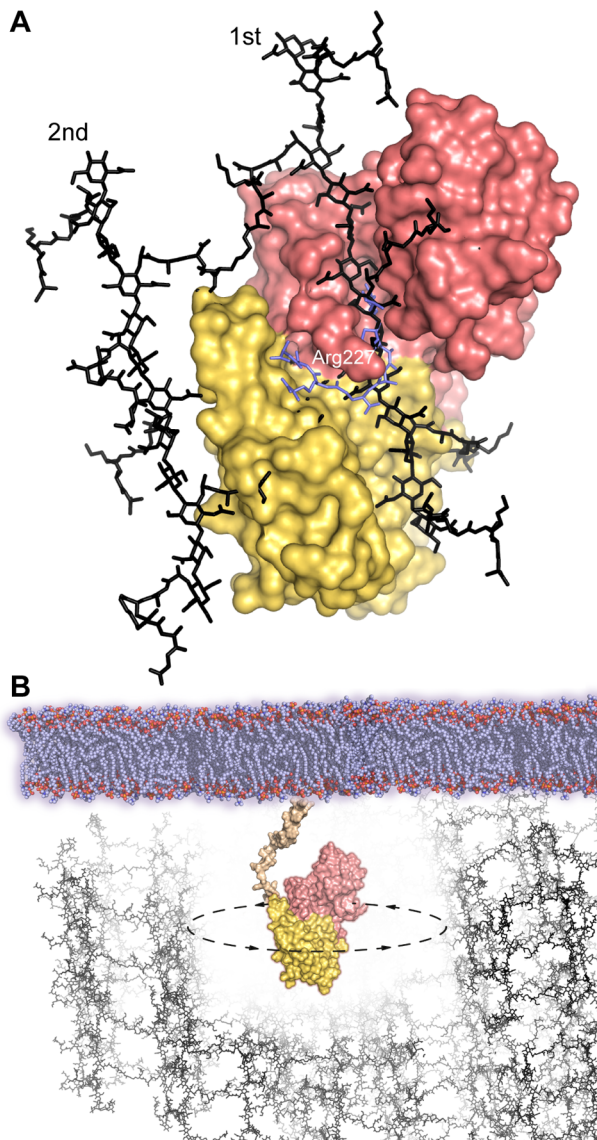


Figure 4. (A) The NMR-based structure of a cross-linked peptidoglycan (in black) is superimposed on the coordinates for the tetrasaccharide from the X-ray structures of the MltC-5 complex (as in Figure 2A). Compound 1 as observed in the MltC-1 complex is represented by blue sticks. Clashes by cross-linked peptide stem are indicated by an arrow. (B) Rotational motion of a single membrane-bound MltC with its disordered linker (residues 19–29, depicted in light brown) could create a large annulus of cleared peptidoglycan.

concave face of the N-terminal domain presents an imposing steric obstacle (Figure 4A).

The requirement for the absence of a cross-link will be reinforced in the living bacterium, as the turgor pressure of the cell renders taut the cross-linked stem peptide. Yet, we identify products with cross-linked peptide stems from the reaction of MltC with the saccus.⁷ This observation is consistent only with the possibility that the neighboring strand of peptidoglycan must be processed by other autolysins *prior* to its recognition by MltC. In this manner, the tautness within that strand due to the turgor pressure is abolished prior to recognition by MltC, and the peptide stem can bind to the surface of the active site. Hence, this is a role for catalysis by MltC. It is a lytic transglycosylase that can only process a strand of peptidoglycan (both in endolytic and exolytic trans-

formations), whose neighboring strand is already turned over by an autolysin.

The role of the N-terminal domain would appear important not as a mere structural extension of the active site beyond what is seen in other lytic transglycosylases but one that creates a peptide-binding site at position +2. As confirmed by our structures and by degradation experiments on purified saccus with the MltC mutants, the occupancy of the peptide-binding site is controlled by Arg227, which allows the enzyme to perform its catalytic activity without detaching from the peptidoglycan chain.

The N-terminal domain of MltC has been designated as DUF3393—Domain of Unknown Function 3393 (Pfam family 11873). Genomic searching revealed that the genomes of 791 bacteria (*Salmonella*, *Shigella*, *Escherichia*, *Yersinia*, *Vibrio*, and *Haemophilus*, among others) encode a lytic transglycosylase having the N-terminal DUF3393 domain (Supporting Information Figure S14). This motif is essentially the entire MltC structure, as studied in the present report. It is likely that this enzyme is more broadly present in bacteria, but the state of the art for analysis of sequences might not be sufficiently sophisticated to identify other homologues, as the sequences diverge. Regardless, the broad presence of MltC (or MltC-like) open-reading frames in various bacteria only argues for the centrality of its biological function to bacteria.

Within the context of our study of reactions and the structure of MltC of *E. coli*, we have disclosed that this enzyme can process a long strand of peptidoglycan once the neighboring cross-linked peptidoglycan is already turned over by other autolysins. In what biological context would this activity be necessary? Intriguing observations have emerged from efforts with MltC homologues. The recent study of Römling et al.²³ directly correlates the MltC activity of *Salmonella enterica* (serovar typhimurium) with the competence to initiate biofilm formation, which (in this organism and numerous other bacteria) correlates to the loss of unencumbered rotation of the flagellum.^{23–26} The unequivocal function of MltC is processing of the cell wall, as disclosed herein. The linkage of this reaction to a functional assembly of flagellum is of note within the context of the structure of MltC. We noted that the stretch of amino acids 19–29 in the MltC structure is disordered. The residue Cys17, just to the N-terminal side of this stretch, is the point of linkage to the membrane via a thioether tether. It is tempting to speculate that the disorder within the residues 19–29 would impart the ability for a rotational motion to MltC to sweep out a large annulus of cleared peptidoglycan per each molecule of enzyme (Figure 4B), which would enable insertion of a large assembly such as that of the flagellum.

METHODS

Cloning of the *mltC* Gene from *E. coli* K12. Genomic DNA from *E. coli* K12 was used as the template for cloning of the full-length *mltC*. The PCR was accomplished using the following primers, *mltC-fw-NdeI* (5'-AGATATA~~C~~ATGACCAAAAAAGGCGATAC-3', with the *NdeI* cut site underlined) and *mltC-rv-XhoI* (5'-CATCTCGAGT~~T~~ATCGCGCGTAGGATTTCGCGGTATT~~C~~-3', with the *XhoI* cut site underlined). The conditions used for the PCR were as follows: 30 cycles of denaturation at 94 °C for 40 s, followed by annealing of primers for 40 s at 60 °C, and extension for 3 min at 72 °C using Pfu DNA polymerase. The reaction volume was 50 μL and contained 0.2 mM triphosphoryldeoxynucleotides (dNTPs), 0.5 μM of each primer, 50 ng of template DNA, and 1 μL of Pfu DNA polymerase. After purification of the PCR product, the fragments were

digested with *Nde*I and *Xba*I and the resulting piece was ligated into a *Nde*I and *Xba*I sites of the T7 expression vector pET-28a-c(+). The recombinant plasmid pET28mltC was constructed and confirmed by sequencing.

Construction of the mltC Mutants. The method from Green and Sambrook²⁷ to create a single specific mutation was used. The method uses four primers and three PCRs to create a site-specific mutation by overlap extension. One pair of primers is used to amplify DNA that contains the mutation site together with upstream sequences. The second pair of primers is used in a separate PCR to amplify DNA that contains the mutation site together with downstream sequences. The mutation is located in the region of overlap and therefore in both amplified fragments. The overlapping fragments are mixed, denatured, and annealed to generate heteroduplexes that can be extended in a third PCR to amplify the full length gene using two primers that bind to the extremes of the fragments. For all the mutants, the pET28mltC plasmid was used as the template DNA and we used the primers mltC-fw-NdeI and mltC-rv-XbaI. In the case of the mltCIS9R mutant, we used the following primers 5'-CTTCAAAAGGTGGCGCGCTGTCCTAAGAC and 5'-GTCCTTAGGACCAGCGCGCACCACTCTTGAGAG. For mltCR227A, primers 5'-AACCGTATGCCGTCAGCGCTTCCGA-TGCGCTGGGATTA and 5'-TAATCCCAGCGCATCG-GAAGCGCTGACCGCATACGGGTT were used. The PCR products were purified and digested as described above, and the recombinant plasmids pET28mltCIS9R and pET28mltCR227A were confirmed by sequencing.

Protein Expressions and Purifications. Colonies containing the construct were selected on LB agar supplemented with 30 mg mL⁻¹ of Kanamycin. Selected cells were incubated overnight in 5 mL of LB medium supplemented with 50 µg mL⁻¹ of Kanamycin. The cells were diluted into 1 L of fresh Kanamycin-supplemented LB medium and growth was continued with agitation (120 rpm) at 37 °C until the culture reached OD₆₀₀ of 0.8. Isopropyl-β-D-thiogalactoside (IPTG) was added at this stage to a concentration of 0.4 mM and the cultures were incubated at 37 °C for an additional 4 h. Cells were harvested by centrifugation, resuspended in 10 mL of 50 mM Tris buffer, pH 8.0, supplemented with 0.3 M NaCl and 20 mM imidazole. Bacteria were disrupted by sonification on ice for 20 cycles of 30 s each with 30 s rest in between cycles. Bacterial debris was removed by centrifugation at 18 000g for 45 min. The supernatant was loaded onto a 5 mL HiTrap Chelating column (GE). The column was washed with 50 mM Tris buffer, pH 8.0, supplemented with 0.3 M NaCl and 20 mM imidazole. Elution was performed using 50 mM Tris buffer, pH 8.0, supplemented with 0.3 M NaCl and 1 M imidazole. The protein was homogeneous by SDS-PAGE. Average molecular masses (M_r)s of purified MltCs (wild type and two mutants) were determined by LC/MS (Supporting Information Table S2).

The protein with His-Tag did not crystallize. Therefore, we removed the His-Tag for the purpose of crystallization by the following procedure. After the Ni-column purification, MltC (32 mg) was dialyzed into 20 mM Tris-HCl, 100 mM NaCl, pH 8.0. We added 320 units of recombinant thrombin to the mixture and allowed the solution to sit at 4 °C during 20 h without shaking, at which time SDS PAGE analysis indicated that the reaction was complete. The sample was run through another Ni-column to retain any traces of unprocessed protein. The processed MltC run through as a single fraction.

Synthesis of Compounds. Compounds 1–6 were prepared according to the literature methods developed by our laboratory.^{13–16}

Reaction of MltC/AmpDh3 with the Bacterial Sacculus and Reaction Products Quantification. MltC (1.7 µM final concentration) was incubated with 100 µL of the sacculus preparation⁷ in 20 mM HEPES, pH 7.0 with 100 mM NaCl and 0.1% Triton X-100 at 37 °C. At various time points (0.5, 2, and 24 h), the reaction was stopped by boiling for 3 min. The reaction mixture was concentrated to dryness, reconstituted in 20 mM phosphate buffer, pH 8.0, and incubated in the presence of AmpDh3 (3 µM final concentration)²⁰ at 37 °C for 5 h. The mixture was boiled for 3 min and was concentrated to dryness. The residue was reduced with sodium borohydride (2 mg)

for 40 min and the reduction reaction was quenched by addition of formic acid. After centrifugation of the resultant suspension (10 min at 14 000g), the supernatant was separated and was used for analysis by LC/MS, according to conditions described previously.²⁰ Briefly, the LC/MS instrument consisted of a Dionex Ultimate 3000 Rapid Separation UPLC system and coupled with a Bruker MicrOTOF-Q II quadrupole time-of-flight hybrid mass spectrometer with electrospray ionization source. Liquid chromatographic separations were achieved by a Dionex Acclaim PolarAdvantage II C18 column (3 µm, 2.1 mm i.d. × 150 mm) using water/acetonitrile (with 0.1% formic acid) as mobile phase. Peak areas from extracted-ion chromatograms of the corresponding *m/z* values were integrated and normalized to the internal standard (compound 5).¹⁶ Total peak areas included the contributions from peak areas of charge states +1, +2, +3, +4, +5, and +6, when present.

Liquid Chromatography/Mass Spectrometry for Determination of Molecular Mass of Purified Proteins. The LC/MS instrument consisted of a Dionex Ultimate 3000 Rapid Separation UPLC system equipped with a Dionex Ultimate 3000 autosampler and a Dionex Ultimate 3000 photodiode array detector coupled with a Bruker MicrOTOF-Q II quadrupole time-of-flight hybrid mass spectrometer using Hystar 3.2 software. The Bruker electrospray ionization source was operated in the positive ion mode with the following parameters: end plate offset voltage = -500 V, capillary voltage = 2000 V, and nitrogen as both a nebulizer (3 bar) and dry gas (6.0 L min⁻¹ flow rate at 200 °C temperature). Mass spectra were accumulated over the mass range 300–3000 Da at an acquisition rate of 5000 per second. Separations were performed on a Phenomenex Aeris wdespore C4 column (3.6 µm, 2.1 mm i.d. × 150 mm). The mobile phase (A = 0.1% formic acid in water; B = 0.1% formic acid in acetonitrile) gradient consisted of elution at 0.3 mL min⁻¹ with 70% A/30% B for 5 min, followed by a 10 min linear gradient to 10% A/90% B, a 0.1 min linear gradient to 70% A/30% B, and then 70% A/30% B for 5 min. Multiply charged ions were deconvoluted using the maximum entropy algorithm.

Crystallization. Native protein MltC was used at 14 mg mL⁻¹, in a buffer of 50 mM tris pH 8, 250 mM NaCl, and 0.1% Triton X-100. Crystals grew in 18% PEG 3350 and 0.2 M triammonium citrate pH 7.5, using the hanging drop vapor-diffusion method at 291 K. The mixture consisted of equal volumes of protein with precipitant solution (1 µL) and equilibrated against 500 µL of the reservoir solution. The crystals were soaked into cryoprotectant solution (20% PEG 400), before flash cooling at 100 K. The complex of MltC with anhydro-disaccharide-pentapeptide (MltC·1) was obtained growing crystals of the protein mutant E217Q at 14 mg mL⁻¹, (in buffer 20 mM Tris pH 7.5, 150 mM NaCl and 0.1% Brij) in the same crystallization condition (18% PEG 3350 and 0.2 M triammonium citrate pH 7.5) and using streak seeding techniques with the native crystals. In order to obtain the complex, these crystals were soaked in a 20 mM solution of compound 1 mixed with the cryoprotectant (20% PEG 400).

The complexes of MltC with tetrasaccharides MltC·5 and MltC·6 were obtained by soaking crystals of MltC E217Q into a 5 mM solution of compound 5 and 6 overnight. Crystals were cryoprotected using 20% PEG 400.

Data Collection and Processing. For the native MltC crystals, 1996 images were collected at the ESRF synchrotron (Grenoble, France), with an oscillation of 0.1° on beamline ID29, using a Pilatus 6 M detector and fixed wavelength of 1.74709 Å. MltC crystallized in the space group P2₁, with unit cell parameters of *a* = 49.87 Å, *b* = 114.65 Å, *c* = 61.40 Å, $\alpha = \gamma = 90^\circ$, $\beta = 93.46^\circ$. Two monomers were found in the asymmetric unit.

For the complex of MltC·1, a complete X-ray diffraction data set of 180 images was collected at the ESRF in beamline ID23-2 using a CCD detector. The oscillation range was of 1.0° and the wavelength was fixed at 0.87260 Å. MltC·1 crystallized in the same space group as the apo form (P2₁), and unit cell parameters were of *a* = 50.16 Å, *b* = 115.0 Å, *c* = 61.28 Å, $\alpha = \gamma = 90^\circ$, $\beta = 93.21^\circ$. All collected images were indexed, integrated and scaled using XDS,²⁸ IMOSFLM and SCALA from CCP4²⁹ program suite. Two monomers were found in the

asymmetric unit. Only in one of these monomers compound **1** was found.

For complexes MltC-**5** and MltC-**6**, a complete X-ray diffraction data set of 1800 images was collected for both complexes at ALBA synchrotron (Barcelona, Spain) in BL13-XALOC beamline, with an oscillation range of 0.2° and a fixed wavelength of 0.97948 Å. A Pilatus 6M detector was used for collection. MltC-**5** crystallized in the space group P2₁, with unit cell parameters of $a = 49.51$ Å, $b = 114.33$ Å, $c = 61.77$ Å, $\alpha = \gamma = 90^\circ$, $\beta = 93.28^\circ$. MltC-**6** also crystallized in space group P2₁, with unit cell parameters of $a = 49.2$ Å, $b = 112.81$ Å, $c = 61.57$ Å, $\alpha = \gamma = 90^\circ$, $\beta = 93.52^\circ$. All collected images were indexed, integrated and scaled using XDS,²⁸ IMOSFLM, and SCALA from CCP4²⁹ program suite, and in both cases, two monomers were found in the asymmetric unit.

Structure Solution and Refinement. MltC apo structure was solved using ARCIIMBOLDO^{17,18} at 2.7 Å resolution (although later on data to at 2.33 Å resolution became available), using fragments of the structure of MltE^{10,11} (2Y8P) that shares a homology of 40% with the C-terminal part of the MltC structure. The best partial solution, characterized by a TFZ score of 7.2 in PHASER,³⁰ was extended in multiple ways adding side chains with SCWRL4³¹ and refined with BUSTER.³² SHELXE³³ was used to apply density modification and autotracing to the refined models, rendering a main-chain trace spanning 352 residues, approximately 50% of the protein contents of the asymmetric unit, and characterized by a CC of 25.77%. The model was manually completed using COOT³⁴ and was refined with PHENIX.³⁵ The R_{work} converged to 0.19 and the R_{free} to 0.26 in the final model. The structure of the complex MltC-**1** was solved by Molecular Replacement (MR) at 2.45 Å resolution, using the native structure of MltC as initial model. MR was done using MOLREP³⁶ and refined with PHENIX.³⁵ Final values of R_{work} and R_{free} are 0.19 and 0.26, respectively.

The rmsd value for the $C\alpha$ of the complex compared to the native structure is 0.48 Å for chain A and 0.41 Å for chain B. The ligand **1** was refined with full occupancy and for both, the native and the complex structure, all of the residues fit perfectly in the Ramachandran plot.

The complex of MltC-**5** was solved by MR at 2.15 Å resolution, using the native structure of MltC as initial model. MR was done using MOLREP³⁶ and refined with PHENIX.³⁵ Final values of R_{work} and R_{free} are 0.19 and 0.27, respectively.

The rmsd value for the $C\alpha$ of the complex MltC-**5** compared to the native structure is 0.43 Å for chain A and 0.23 Å for chain B. The ligand **5** was refined with full occupancy.

The third complex of MltC-**6** was solved using MR at 2.9 Å resolution, using the native structure of MltC as initial model. MR was done using MOLREP³⁶ and refined with PHENIX.³⁵ Final values of R_{work} and R_{free} are 0.16 and 0.25, respectively.

The rmsd value for the $C\alpha$ of the complex MltC-**6** compared to the native structure is 0.53 Å for chain A and 0.65 Å for chain B. The ligand **6** was refined with full occupancy.

Data refinement results and statistics are summarized in Table 1.

Energy Minimization for Disaccharide Moiety of Ligand **1.** The crystal structure was prepared using Maestro,³⁷ during which, bond orders were assigned and hydrogen atoms were added to the protein. Energy minimization was carried out with Desmond.³⁸ The structure was solvated with an orthorhombic box of water molecules of 10 Å buffer size from the protein surface using TIP4P water model. Chloride ions were added to neutralize the system. The entire system was energy minimized employing a hybrid method of unconstrained steepest descent, followed by limited-memory Broyden–Fletcher–Goldfarb–Shanno (LBFGS) algorithm with a convergence threshold gradient of 0.5 kcal/mol.

ASSOCIATED CONTENT

Supporting Information

Supplemental tables and figures. This material is available free of charge via the Internet at <http://pubs.acs.org>.

Accession Codes

The crystallographic coordinates are deposited in the Protein Data Bank (PDB codes 4CSF, 4CHX, 4CFP, and 4CFO for MltC, MltC-**1** complex, MltC-**5** complex and MltC-**6** complex, respectively).

AUTHOR INFORMATION

Corresponding Authors

*Email: mobashery@nd.edu.

*Email: xjuan@iqfr.csic.es.

Author Contributions

[†]C.A.-R. and M.L. contributed equally.

Notes

The authors declare no competing financial interest.

ACKNOWLEDGMENTS

We thank the staff from ESRF and ALBA synchrotron beamlines for help in data collection. This work was supported by a grant from the US National Institutes of Health (GM61629) and by grants BFU2011-25326 (the Spanish Ministry of Economy and Competitiveness) and S2010/BMD-2457 (the Government of Community of Madrid). K.M. is grateful for a Juan de la Cierva grant. I.U. is grateful to the Spanish MINECO and Generalitat de Catalunya for financial support (IDC-20101173 and 2009SGR-1036). The Mass Spectrometry & Proteomics Facility of the University of Notre Dame is supported by grant CHE0741793 from the National Science Foundation.

REFERENCES

- (1) Fisher, J. F., and Mobashery, S. (2010) Host–guest chemistry of the peptidoglycan. *J. Med. Chem.* 53, 4813–4829.
- (2) Park, J. T., and Uehara, T. (2008) How bacteria consume their own exoskeletons (turnover and recycling of cell wall peptidoglycan). *Microbiol. Mol. Biol. Rev.* 72, 211–227.
- (3) Suvorov, M., Fisher, J. F., Mobashery, S. (2009) Bacterial Cell Wall: Morphology and Biochemistry. In *Practical Handbook of Microbiology*, 2nd ed.; Goldman, E.; Green, L. H., Eds.; CRC Press, Boca Raton, FL.
- (4) Scheurwater, E., Reid, C. W., and Clarke, A. J. (2008) Lytic transglycosylases: Bacterial space-making autolysins. *Int. J. Biochem. Cell Biol.* 40, 586–591.
- (5) van Heijenoort, J. (2011) Peptidoglycan hydrolases of *Escherichia coli*. *Microbiol. Mol. Biol. Rev.* 75, 636–663.
- (6) Scheurwater, E. M., and Clarke, A. J. (2008) The C-terminal domain of *Escherichia coli* YfhD functions as a lytic transglycosylase. *J. Biol. Chem.* 283, 8363–8373.
- (7) Lee, M., Hesek, D., Llarrull, L. I., Lastochkin, E., Pi, H., Boggess, B., and Mobashery, S. (2013) Reactions of all *Escherichia coli* lytic transglycosylases with bacterial cell wall. *J. Am. Chem. Soc.* 135, 3311–3314.
- (8) van Straaten, K. E., Dijkstra, B. W., Vollmer, W., and Thunnissen, A. M. (2005) Crystal structure of MltA from *Escherichia coli* reveals a unique lytic transglycosylase fold. *J. Mol. Biol.* 352, 1068–1080.
- (9) van Asselt, E. J., Dijkstra, A. J., Kalk, K. H., Takacs, B., Keck, W., and Dijkstra, B. W. (1999) Crystal structure of *Escherichia coli* lytic transglycosylase Slt35 reveals a lysozyme-like catalytic domain with an EF-hand. *Structure* 7, 1167–1180.
- (10) Artola-Recolons, C., Carrasco-Lopez, C., Llarrull, L. I., Kumarasiri, M., Lastochkin, E., Martinez de Ilarduya, I., Meindl, K., Uson, I., Mobashery, S., and Hermoso, J. A. (2011) High-resolution crystal structure of MltE, an outer membrane-anchored endolytic peptidoglycan lytic transglycosylase from *Escherichia coli*. *Biochemistry* 50, 2384–2386.

- (11) Fibriansah, G., Gliubich, F. I., and Thunnissen, A. M. (2012) On the mechanism of peptidoglycan binding and cleavage by the endo-specific lytic transglycosylase MltE from *Escherichia coli*. *Biochemistry* 51, 9164–9177.
- (12) van Asselt, E. J., Thunnissen, A. M., and Dijkstra, B. W. (1999) High resolution crystal structures of the *Escherichia coli* lytic transglycosylase Slt70 and its complex with a peptidoglycan fragment. *J. Mol. Biol.* 291, 877–898.
- (13) Hesek, D., Lee, M., Zhang, W., Noll, B. C., and Mobashery, S. (2009) Total synthesis of N-acetylglucosamine-1,6-anhydro-N-acetyl-muramylpentapeptide and evaluation of its turnover by AmpD from *Escherichia coli*. *J. Am. Chem. Soc.* 131, 5187–5193.
- (14) Lee, M., Zhang, W., Hesek, D., Noll, B. C., Boggess, B., and Mobashery, S. (2009) Bacterial AmpD at the crossroads of peptidoglycan recycling and manifestation of antibiotic resistance. *J. Am. Chem. Soc.* 131, 8742–8743.
- (15) Lee, M., Hesek, D., Shah, I. M., Oliver, A. G., Dworkin, J., and Mobashery, S. (2010) Synthetic peptidoglycan motifs for germination of bacterial spores. *ChemBioChem* 11, 2525–2529.
- (16) Martinez-Caballero, S., Lee, M., Artola-Recolons, C., Carrasco-Lopez, C., Hesek, D., Spink, E., Lastochkin, E., Zhang, W., Hellman, L. M., Boggess, B., Mobashery, S., and Hermoso, J. A. (2013) Reaction products and the X-ray structure of AmpDh2, a virulence determinant of *Pseudomonas aeruginosa*. *J. Am. Chem. Soc.* 135, 10318–10321.
- (17) Rodriguez, D. D., Grosse, C., Himmel, S., Gonzalez, C., de Ilarduya, I. M., Becker, S., Sheldrick, G. M., and Uson, I. (2009) Crystallographic *ab initio* protein structure solution below atomic resolution. *Nat. Methods* 6, 651–653.
- (18) Rodriguez, D., Sammito, M., Meindl, K., de Ilarduya, I. M., Potratz, M., Sheldrick, G. M., and Uson, I. (2012) Practical structure solution with ARCIMBOLDO. *Acta Crystallogr., Sect. D: Biol. Crystallogr.* 68, 336–343.
- (19) Holm, L., and Rosenstrom, P. (2010) Dali server: Conservation mapping in 3D. *Nucleic Acids Res.* 38, 545–549.
- (20) Lee, M., Artola-Recolons, C., Carrasco-Lopez, C., Martinez-Caballero, S., Hesek, D., Spink, E., Lastochkin, E., Zhang, W., Hellman, L. M., Boggess, B., Hermoso, J. A., and Mobashery, S. (2013) Cell wall remodeling by the zinc-protease AmpDh3 from *Pseudomonas aeruginosa*. *J. Am. Chem. Soc.* 135, 12604–12607.
- (21) Zhang, W., Lee, M., Hesek, D., Lastochkin, E., Boggess, B., and Mobashery, S. (2013) Reactions of the three AmpD enzymes of *Pseudomonas aeruginosa*. *J. Am. Chem. Soc.* 135, 4950–4953.
- (22) Meroueh, S. O., Bencze, K. Z., Hesek, D., Lee, M., Fisher, J. F., Stemmler, T. L., and Mobashery, S. (2006) Three-dimensional structure of the bacterial cell wall peptidoglycan. *Proc. Natl. Acad. Sci. U.S.A.* 103, 4404–4409.
- (23) Monteiro, C., Fang, X., Ahmad, I., Gomelsky, M., and Romling, U. (2011) Regulation of biofilm components in *Salmonella enterica* serovar Typhimurium by lytic transglycosylases involved in cell wall turnover. *J. Bacteriol.* 193, 6443–6451.
- (24) Belas, R., Zhulin, I. B., and Yang, Z. (2008) Bacterial signaling and motility: Sure bets. *J. Bacteriol.* 190, 1849–1856.
- (25) Duan, Q., Zhou, M., Zhu, L., and Zhu, G. (2013) Flagella and bacterial pathogenicity. *J. Basic Microbiol.* 53, 1–8.
- (26) Guttenplan, S. B., and Kearns, D. B. (2013) Regulation of flagellar motility during biofilm formation. *FEMS Microbiol. Rev.* 37, 849–871.
- (27) Green, M. R., and Sambrook, J. (2012) *Molecular Cloning: A Laboratory Manual*, 4th ed.; Cold Spring Harbor Laboratory Press, Cold Spring Harbor, NY.
- (28) Kabsch, W. (2010) XDS. *Acta Crystallogr., Sect. D: Biol. Crystallogr.* 66, 125–132.
- (29) Winn, M. D., et al. (2011) Overview of the CCP4 suite and current developments. *Acta Crystallogr., Sect. D: Biol. Crystallogr.* 67, 235–242.
- (30) McCoy, A. J., Grosse-Kunstleve, R. W., Adams, P. D., Winn, M. D., Storoni, L. C., and Read, R. J. (2007) Phaser crystallographic software. *J. Appl. Crystallogr.* 40, 658–674.
- (31) Krivov, G. G., Shapovalov, M. V., and Dunbrack, R. L., Jr. (2009) Improved prediction of protein side-chain conformations with SCWRL4. *Proteins* 77, 778–795.
- (32) Bricogne, G., Blanc, E., Brandl, M., Flensburg, C., Keller, P., Paciorek, W., Roversi, P., Sharff, A., Smart, O. S., Vonrhein, C., and Womack, T. O. (2011) BUSTER version X.Y.Z., Global Phasing Ltd, Cambridge, U.K.
- (33) Sheldrick, G. M. (2010) Experimental phasing with SHELXC/D/E: combining chain tracing with density modification. *Acta Crystallogr., Sect. D: Biol. Crystallogr.* 66, 479–485.
- (34) Emsley, P., and Cowtan, K. (2004) Coot: Model-building tools for molecular graphics. *Acta Acta Crystallogr., Sect. D: Biol. Crystallogr.* 60, 2126–2132.
- (35) Adams, P. D., Afonine, P. V., Bunkoczi, G., Chen, V. B., Davis, I. W., Echols, N., Headd, J. J., Hung, L. W., Kapral, G. J., Grosse-Kunstleve, R. W., McCoy, A. J., Moriarty, N. W., Oeffner, R., Read, R. J., Richardson, D. C., Richardson, J. S., Terwilliger, T. C., and Zwart, P. H. (2010) PHENIX: A comprehensive Python-based system for macromolecular structure solution. *Acta Crystallogr., Sect. D: Biol. Crystallogr.* 66, 213–221.
- (36) Vagin, A., and Teplyakov, A. (1997) MOLREP: An automated program for molecular replacement. *J. Appl. Crystallogr.* 30, 1022–1025.
- (37) Maestro, version 9.4 (2013), Schrödinger, Inc., New York.
- (38) Bowers, K. J., Chow, E., Xu, H., Dror, R. O., Eastwood, M. P., GregerSEN, B. A., Klepeis, J. L., Kolossvary, I., Moraes, M. A., and Sacerdoti, F. D. (2006) *Proceedings of the ACM/IEEE*, Vol. 43; IEEE, New York.